ELSEVIER

Nuclear Instruments and Methods in Physics Research A 469 (2001) 147–158

NUCLEAR INSTRUMENTS & METHODS IN PHYSICS RESEARCH Section A

www.elsevier.com/locate/nima

Cluster shapes and cluster sizes in the HERA-B silicon vertex detector

I. Abt[a], C. Bauer[b], M. Bräuer[b], M. Dressel[a], T. Glebe[b], T. Jagla[b], I. Kisel[a], K.T. Knöpfle[b], S. Masciocchi[a], T. Perschke[a], V. Pugatch[b], M. Sang[a], S. Schaller[a], M. Schmelling[b], B. Schwingenheuer[b], F.G. Sciacca[b], E. Sexauer[b], U. Trunk[b], W. Wagner[a,*], R. Wanke[b]

[a] *Max-Planck-Institut für Physik, Föhringer Ring 6, 80805 München, Germany*
[b] *Max-Planck-Institut für Kernphysik, Postfach 10 39 80, 69029 Heidelberg, Germany*

Received 20 November 2000

Abstract

We report on investigations of shape and size of the clusters on the silicon detectors of the HERA-B vertex detector. The data taken during the commissioning run of 1999 are compared to predictions of model calculations.

PACS: 29.40.Wk; 29.40.Gx

Keywords: Silicon detector; Cluster shape; Cluster size

1. Introduction

HERA-B is a fixed target experiment at the HERA proton storage ring located at the DESY laboratory in Hamburg. The main objective is to measure CP violation in neutral B meson decays [1]. HERA-B is designed as a forward spectrometer with particle identification. Proton–nucleon interactions are produced with an internal wire target at a rate of 40 MHz. About 10^6 inelastic interactions yield one $b\bar{b}$ pair.

The vertex detector system (VDS) of HERA-B provides precision tracking information to reconstruct primary vertices at the target and secondary decay vertices. The B mesons produced in HERA-B have a mean decay length of 11.8 mm. The vertex detector is based on 64 double-sided silicon microstrip detectors which are mounted in eight planes, the so-called superlayers, perpendicular to the beam axis. Each superlayer is segmented into four quadrants with two double-sided detectors each. The system covers an angular acceptance from 10 to 250 mrad in the lab frame. The silicon detectors in the first seven superlayers are mounted

*Corresponding author. Universität Karlsruhe, Institut für Experimentelle Kernphysik (EKP), Wolfgang-Gaede-Straße 1, 76128 Karlsruhe, Germany. Tel.: +49-721-608-4706.

E-mail address: wagner@ekp.physik.uni-karlsruhe.de (W. Wagner).

0168-9002/01/$ - see front matter
PII: S0168-9002(01)00775-6

inside Roman pots housed in a 2.6 m long vacuum vessel. The pots are movable in the radial and lateral directions to the beam. Thereby the pots can be moved close to the beam for data taking and remain retracted otherwise. The 8th superlayer is mounted stationary on the exit window of the vessel.

The microstrip detectors were designed by the Halbleiterlabor (HLL) of the Max-Planck-Institutes in Munich [2–4]. Detectors were produced at HLL and SINTEF (Oslo, Norway) [5]. The silicon sensors are based on a 280 μm thick n-type sub-strate and have an active area of $50 \times 70\ \mathrm{mm}^2$. The implanted strips on the n-side (n^+-strips) of the detector are orthogonal to those on the p-side (p^+-strips). However, the strips are tilted by 2.5° with respect to the corresponding detector edge. Thereby a stereo angle of 5° is achieved when two detectors are mounted back-to-back in one quadrant. Thus, each superlayer provides four stereo views: ±2.5°, 87.5° and 92.5°, which allows independent track finding inside the VDS.

Geometric optimization yields a readout pitch of 54.67 μm on the n-side and 51.75 μm on the p-side. On the n-side there are 1280 readout strips, on the p-side 1024. The detectors are AC coupled, feature polysilicon bias resistors and multi-guardring structures. On the n-side two different techniques are used to insulate the n^+-strips: a moderated p-spray (HLL) or p-stop (SINTEF) implantation. On the n-side of the p-spray detectors and on all p-sides there is an additional intermediate implanted strip between two readout strips. On the p-stop detectors these intermediate strips are omitted, since there is not enough space available. More detailed information on the vertex detector system and the silicon detectors can be found in Refs. [4,6–9].

The HERA-B vertex detector was fully equipped in 1999 and commissioned in 1999 and 2000. Part of the commissioning was the analysis of cluster shapes and cluster sizes which is presented in this paper. One aim was to investigate the influence of the selection cuts on these distributions and describe the observations by a model. The other aim was to verify predictions derived from data taken with a laser test stand [14] and thereby proof the usability of laser tests for studies of silicon detectors.

2. Raw data processing and cluster search

The silicon detectors are read out using HELIX128 [10] analog readout-chips which comprise 128 channels each. Each readout channel features an analog pipeline for a latency of 128 bunch crossings (BX). The chips are operated with a sampling frequency of 10.4 MHz which is determined by the BX-frequency of the HERA proton ring. When a trigger is received, the multiplexed analog output from the requested pipeline cell is transferred via optical links to front end boards where the signals are digitized and stored in memory for further processing. The readout frequency is 20.8 MHz.

As a first step pedestals are subtracted. Since the pedestals drift slowly with time, a pedestal and noise following procedure is employed. As a second step a chipwise common mode fit is performed. For the common mode fit, a first order spline interpolation is used. The clusters on the detectors are selected by cutting on two quantities: the strip significance t_i and the cluster significance T:

$$t_i(n) = q_i^2(n)/v_i(n) \quad \text{and} \quad T = \sum_{j=k}^{j=k+m-1} q_j^2(n)/v_j(n) \tag{1}$$

where $q_i(n)$ is the charge—the pulse height after pedestal and common mode subtraction—on strip number i for the event n. v_i is the variance of the pedestal of strip i. The noise is therefore given by $\sqrt{v_i}$. Firstly, strips whose strip significance exceeds a threshold t_0 are selected. Neighboring strips above threshold are merged into one cluster. The cluster width is denoted by m and gives the number of strips in a cluster. In Eq. (1) we write k for the strip number of the first strip of a cluster. The cluster significance T must be above a threshold T_0 for the cluster to be accepted. During standard operation sparsified data, containing only information on the accepted clusters, is written to tape.

After the selection step, the clusters are handed over to the tracking program. Two different packages are available: CATS [11,12] and HOLMES [13]. CATS is based on a Cellular Automaton and HOLMES on a Kalman filter approach. We used CATS for tracking in the study presented in this paper. In the cluster analysis only those clusters were used which were associated with a track.

An important measure for the quality of the employed silicon detectors is the signal-to-noise ratio (S/N). We use the following definition of this quantity:

$$S/N = \frac{\sum_{j=k}^{j=k+m-1} q_j}{\sqrt{\sum_{j=k}^{j=k+m-1} v_j}}\sqrt{m}. \quad (2)$$

3. The shape of two-strip clusters

In this paper the discussion of cluster shapes is restricted to the easiest case, to two-strip clusters. The shape of a two-strip cluster consisting of the strips with number n and $n+1$ is described by the parameter η which gives the fractional charge seen on strip $n+1$:

$$\eta = \frac{q_{n+1}}{q_n + q_{n+1}}. \quad (3)$$

In this analysis the η-parameter is calculated for each two-strip cluster associated to a track. The values of η are histogrammed separately for each detector side. The η-distributions are normalized such that the integral is equal to 100. The bin width is 0.01.

Examples of distributions for two detector n-sides are shown in Fig. 1, one with intermediate strips (Fig. 1a) and one without (Fig. 1b). In the first case there are three peaks visible in the distribution: one for readout strip n, one for the intermediate strip and one for the readout strip $n+1$. In the latter case the central peak corresponding to the intermediate strip is missing.

The plots in Fig. 1 were obtained from a run in which the detector n-sides were centered with respect to the proton beam, a configuration which is schematically depicted in Fig. 2a. However, the standard operation mode in HERA-B is an asymmetric configuration as illustrated in Fig. 2b. In this case the η-distributions show certain asymmetries as can be seen from Fig. 3.

The observed asymmetries are due to tracks having a non-perpendicular inclination angle with respect to the silicon wafers and to transverse diffusion of the generated charge carriers. This effect is demonstrated in Fig. 4. A charged particle generates a cloud of free charge carriers (electrons and holes) along its track. Due to the electric field inside the bulk of the detector the charges drift

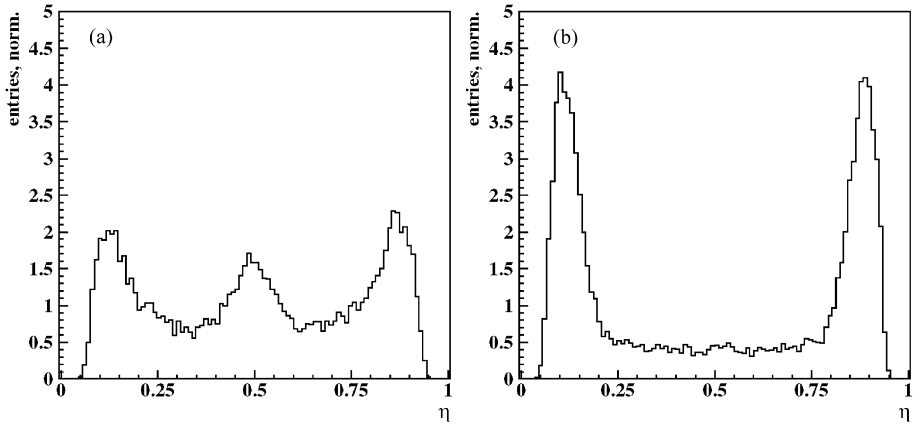

Fig. 1. η-distributions for detector n-sides with intermediate strip, (a), and without intermediate strip, (b). Used cuts: $t_i > 2.0$ and $T > 20.0$.

towards the implantations at the surface. During the drift process the charge distribution spreads in the transverse direction due to diffusion. The longer the drift distance the stronger the diffusion and the wider is the charge distribution when reaching the readout strips. This effect is explained in more detail by a model which is presented in Section 5. The model is used to make predictions for the η-distributions.

The correlation between tracks having a non-perpendicular inclination angle and the rise of the asymmetry is shown in Fig. 5. The histograms are generated using the same data as in Fig. 1, but only those clusters are used which are associated to tracks with an inclination angle $\theta_y < -20$ mrad (Fig. 5a and c) or $\theta_y > 20$ mrad (Fig. 5b and d), respectively. These distributions show asymmetries which are mirrored for hits connected to tracks with negative or positive inclination angles, respectively.

If the n-sides are centered as shown in Fig. 2a, one has approximately the same number of tracks with positive as with negative inclination angle and the asymmetry cancels in the combined histogram (see Fig. 1). If the n-sides are operated in an asymmetric configuration as in Fig. 2b one type of tracks, e.g. with positive inclination angle, dominates and an asymmetry in the η-distribution arises (see Fig. 3).

On the p-sides the asymmetry is always there, since all tracks have the same inclination with respect to the p-side strips independent from the lateral position of the detector. Typical distributions on the p-side of two detectors mounted back-

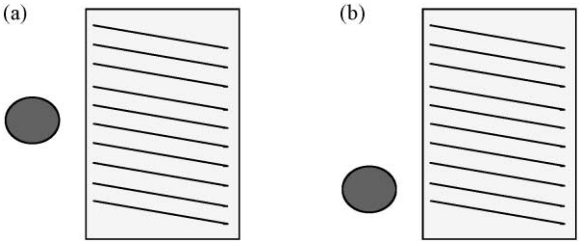

Fig. 2. Different positions of the silicon detectors with respect to the beam. (a) Centered position, in which the η-distributions show no asymmetry. (b) Standard position, in which asymmetries occur.

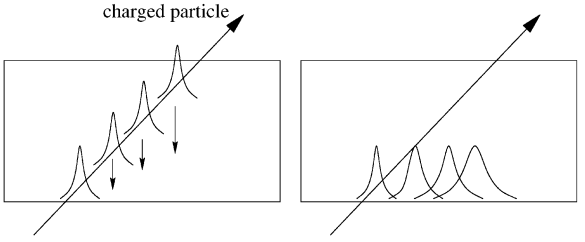

Fig. 4. Schematical explanation for the asymmetry of the charge distribution at the readout strips for tracks with a non-perpendicular inclination angle.

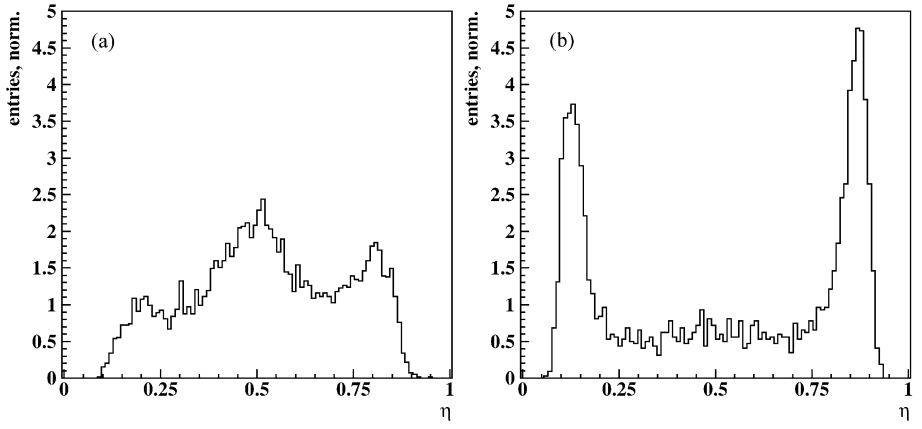

Fig. 3. Asymmetric η-distribution for detector n-sides with intermediate strip, (a), and without intermediate strip, (b). Used cuts: $t_i > 5$ and $T > 15$. Plots taken from Ref. [15].

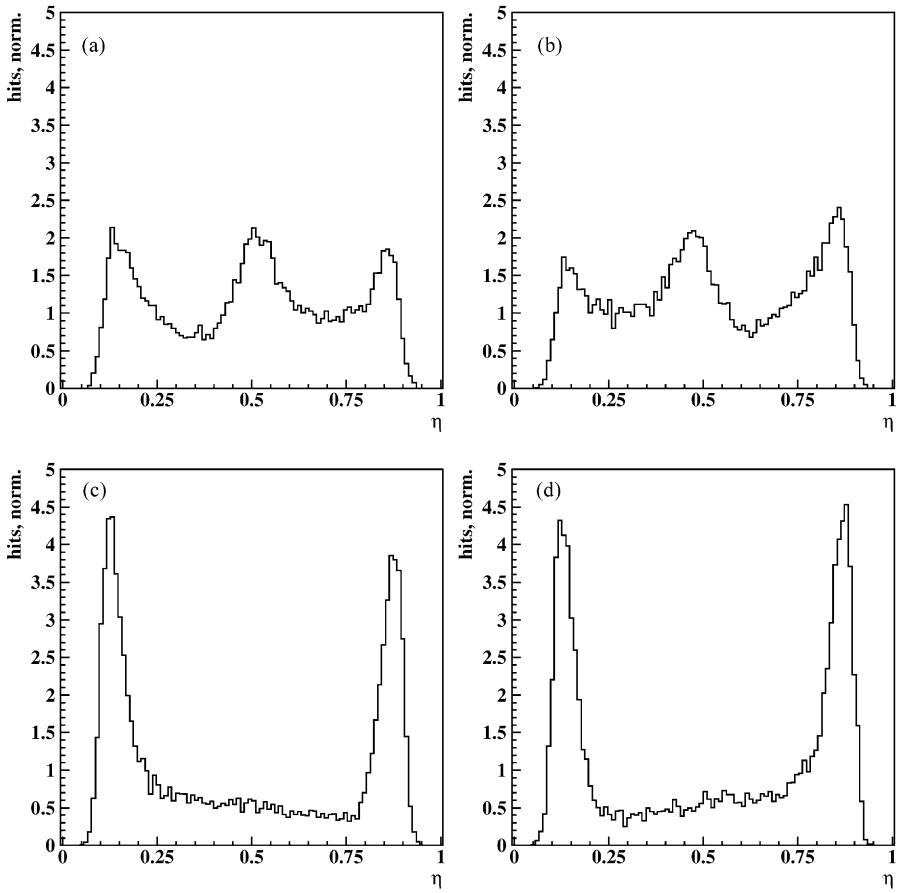

Fig. 5. η-distributions for detector n-sides with intermediate strip, (a) and (b), and without intermediate strip, (c) and (d). The plots in (a) and (c) contain only hits from tracks with an inclination angle of $\theta_y < -20$ mrad. In (b) and (d) the hits stem from tracks with $\theta_y > 20$ mrad.

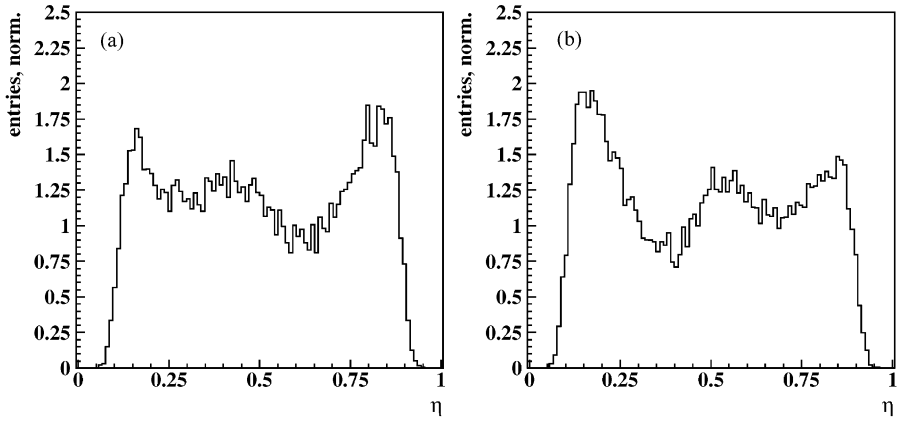

Fig. 6. η-distribution for detector p-sides. (a) and (b) show the distributions of the p-sides of two modules mounted back-to-back.

to-back in one quadrant are shown in Fig. 6. The expected flip of the asymmetry between the two sides is observed.

4. Using η-distributions to estimate the spatial hit resolution

From the measured η-distributions $n(\eta)$ one can derive an η-curve which establishes a relation between a particular η-value and the reconstructed coordinate x_{rec}. The coordinate $x_{\mathrm{rec}}(M)$ is obtained by integrating over the η-bins up to bin number M. This method assumes that the particles are uniformly distributed over the distance of one strip pitch. Despite the highly non-uniform flux in HERA-B this assumption is still true up to 1% due to the small readout pitch of about 50 μm. For $x_{\mathrm{rec}}(M)$ we obtain the relation:

$$x_{\mathrm{rec}}(M) = x_0 + \frac{0.9h}{N_0}\sum_{i=1}^{i=M} n(\eta_i) \quad \text{with } M = 1,\ldots,100. \tag{4}$$

In this formula, h is the readout pitch and N_0 is the number of events in the η-distribution. η_i is the value of bin i in the η-distribution. x_0 is a shift of the origin to take into account that there are no events with $\eta < 0.05$ or $\eta > 0.95$ in the η-distributions. This is due to the selection cuts. Clusters from particles which go through one of the readout strips are mostly recognized as 1-strip or 3-strip clusters. For the same reason we added the factor 0.9 in Eq. (4).

Applying Eq. (4) to the distributions in Fig. 1 we get the η-curves in Fig. 7a and b. The origin shift was adjusted to $x_0 = 3$ μm. In HERA-B the particle impact point x_{est} is estimated by calculating the center of charge. For 2-strip clusters this is equivalent to multiplying the η value with the readout pitch. The error of this method is estimated by calculating the difference $\Delta x = x_{\mathrm{rec}} - x_{\mathrm{est}}$, which is shown in Fig. 7c and d. The mean of these differences is $\bar{\Delta x}_{\mathrm{ims}} = 1$ μm (with intermediate strip) and $\bar{\Delta x}_{\mathrm{wims}} = 5$ μm (without intermediate strip). These values give an estimate on the spatial hit resolution on our detectors and substantiate our decision to employ detectors with intermediate strips.

5. Modeling η-distributions

A model to describe the signal formation and charge division within our silicon strip detectors was already presented in earlier publications [14,15]. This model was used to explain charge division measurements taken with a laser test stand. The drift process, transverse diffusion and the capacitive coupling between the detector strips were taken into account (see Refs. [14,15] for more detailed information on those issues). The existing model was extended to predict η-distributions and explain the observed asymmetries in Fig. 3. We additionally incorporate the modeling of primary charge distributions generated by particles which traverse the detectors non-perpendicularly.

Fig. 8a–d illustrate the model calculations: The charge distribution at the readout strips is given by a superposition of Gaussian charge distributions of different widths (due to transverse diffusion) and different peak position (due to the inclination angle), as indicated in Fig. 8a. The diffusion width Δx_{diff} is given in Fig. 8b as a function of the depth where the primary charges are generated (solid line: electrons drifting to the n-side; dashed line: holes drifting to the p-side).

To take the non-perpendicular inclination angle into account we use a certain spread $\Delta x_{\mathrm{peak}}(\theta)$ of the peak positions of the Gaussian distributions. The spread Δx_{peak} is a function of the inclination angle θ of the track with respect to the projection coordinate of the detector strips: $\Delta x_{\mathrm{peak}}(\theta) = \tan(\theta)b$, where $b = 280$ μm is the detector depth. In the simulation we integrate over 10 different values for Δx_{peak} ranging from 0 to 20 μm. We account for the angular distribution of the tracks by assigning a weight w_θ to each value of Δx_{peak}. The weight distribution is approximated by a linear relation between w_θ and Δx_{peak}: $w_\theta = 5 - 0.23\Delta x_{\mathrm{peak}}$.

Fig. 8c shows the resulting charge distribution at the readout strips given by the superposition shown in Fig. 8a. This distribution is obviously asymmetric, even though its center of charge

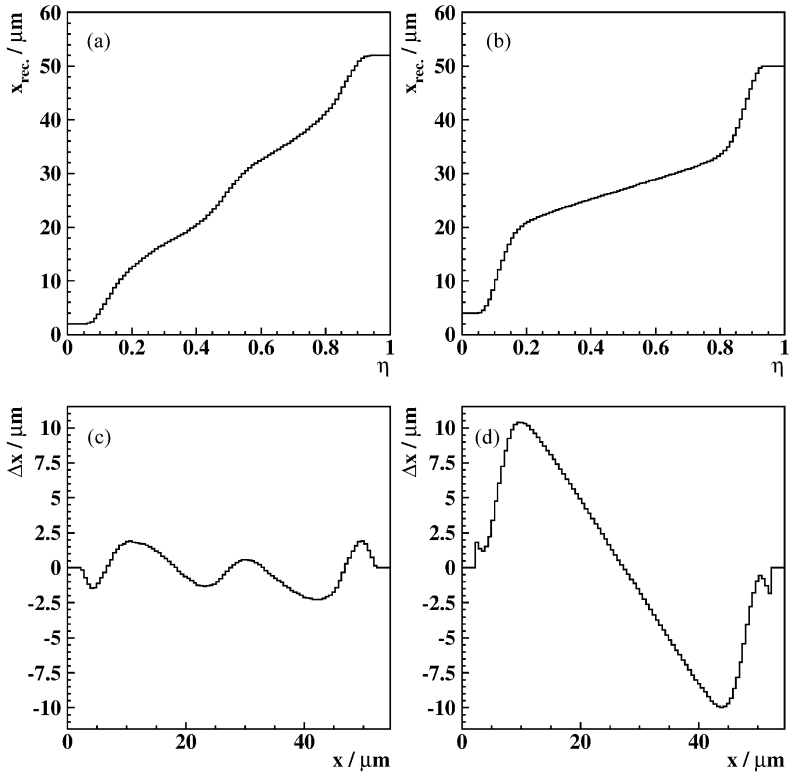

Fig. 7. Estimation of the spatial hit resolution. Using (4) calculates x_{rec} from the distributions in Fig. 1; (a) for a detector with intermediate strip, (b) without intermediate strip. (c) and (d) shows $\Delta x = x_{rec} - x_{est}$.

remains at the origin. Within the model this charge distribution acts on a strip pattern and the fractional charges collected at the readout strips are calculated. These fractions are scaled by all possible signal-to-noise values from 10 to 100 (with a binning of 1) and then compared to a threshold. Neighboring strips which pass this cut are merged to form a cluster. Two-strip clusters are used to calculate the η-parameter according to (3). Clusters of other widths (1-strip, 3-strips, or more) are discarded.

One has to take into account that the different signal-to-noise values do not occur with the some probability, but are rather distributed according to a Landau distribution. This is done by assigning a weight $w_{s/n}$ to each accepted η-value according to the Landau distribution of the signal-to-noise which is obtained from a fit to real data. Fig. 8d shows those Landau distributions used to obtain the results in Fig. 8e (solid line in Fig. 8d) and Fig. 8f (dashed line in Fig. 8d). When filling the η-values into a histogram we use a combined weight $w = w_\theta w_{s/n}$.

The η-distributions predicted by the model to fit the real data of Fig. 3 are shown in Fig. 8e (with intermediate strip, compare Fig. 3a) and Fig. 8f (without intermediate strip, compare Fig. 3b). The asymmetry of the measured distributions in Fig. 3 is clearly reproduced. The same model used to describe laser data can also predict data originating from minimum ionizing particles and thus we are confident that further laser studies will allow realistic tests of our silicon strip detectors. Future studies will mainly deal with investigations of irradiated detectors.

6. Cluster shapes for different selection cuts

The influence of the selection cuts for clusters on the cluster shape distributions (η-distributions)

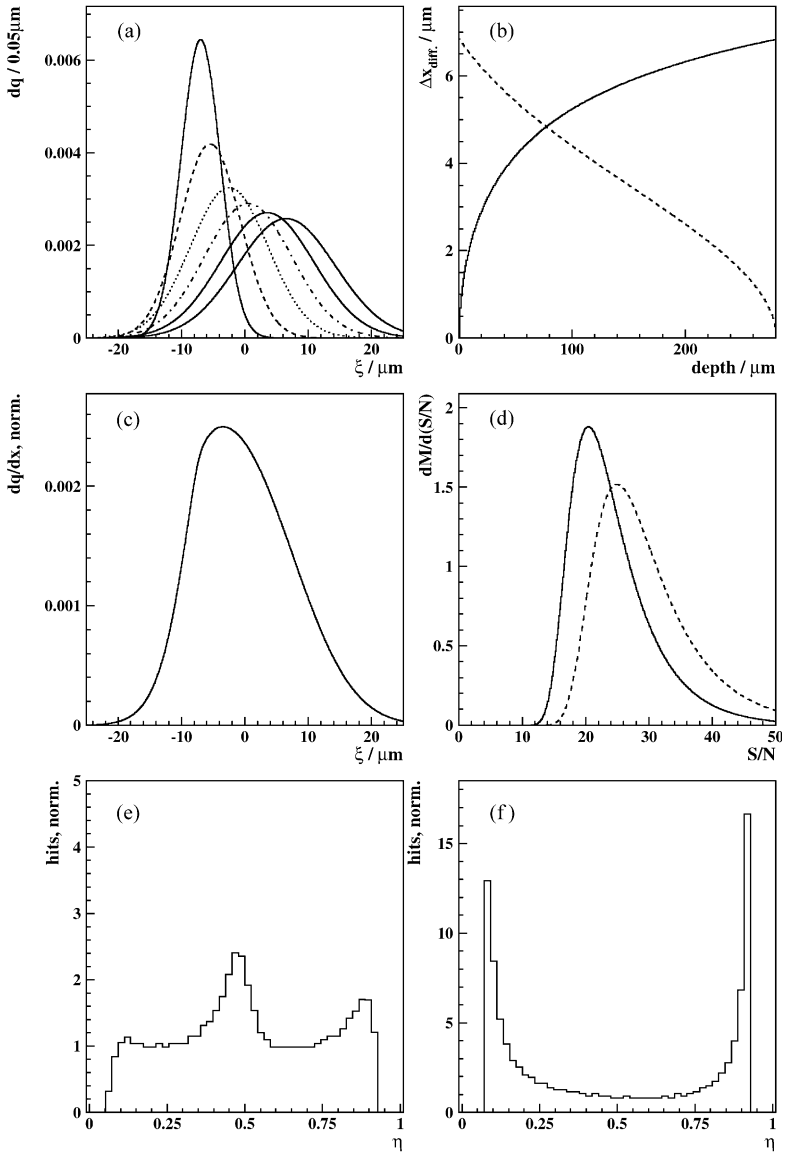

Fig. 8. Model illustration: (a)–(d) illustrate the model to explain the η-distributions, in particular the asymmetry of these distributions: (a) Gaussian distributions of different widths are superimposed to obtain the charge distribution at the readout strips shown in (c). The diffusion width Δx_{diff} of the Gaussian curves is given in (b) as a function of the depth where the primary charge carrier was generated (solid curve for electrons, dashed curve for holes). The Gaussian curves are normalized such that they cover the same area. The η-values are weighted according to the signal-to-noise distributions of the detectors shown in (d) (solid line: used to obtain η-distribution in (e); dashed line: used to obtain η-distribution in (f)). Model results: (e) and (f) show the predictions of the model for those data shown in Fig. 3. (e) n-side with intermediate (Fig. 3a). (f) n-side without intermediate strip (Fig. 3b).

was studied. The cut on the cluster significance T has negligible impact on the distributions, while the cut on the strip significance t_i causes differences in the distributions, as illustrated in Fig. 9.

The higher the cut on t_i the softer are the edges of the η-distribution. The reason for this is that many two-strip clusters are accepted only as one-strip clusters when going to higher thresholds.

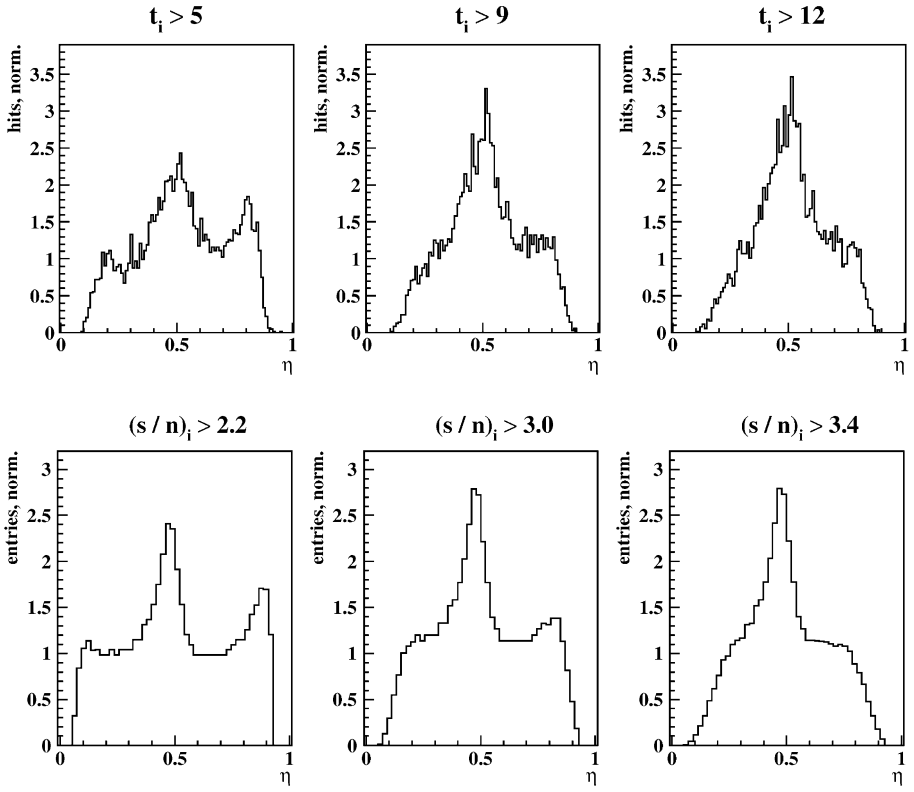

Fig. 9. η-distributions for different selection cuts on the strip significance t_i from real data (upper row) and from the model (lower row). The cut on the cluster significance for real data was $T > 15$. The variation with the T-threshold is marginal and therefore not shown. The angular distribution of tracks used in the simulation is the same as described in Section 5. We assume the relation $(s/n)_i = \sqrt{t_i}$ to compare real and simulated data.

Table 1
Cluster widths distributions for two double-sided detectors. n-sides: n1 (with intermediate strips), n2 (without intermediate strips). p-sides: p1, p2

Side	t_i	1 strip	2 strips	3 strips	4 strips	5 strips	$\geqslant$6 strips
n1	$t_i > 2$	5%	31%	39%	18%	5%	2%
n1	$t_i > 5$	13%	51%	27%	7%	1%	1%
n2	$t_i > 2$	6%	31%	47%	12%	2%	2%
n2	$t_i > 5$	19%	46%	29%	4%	1%	1%
p1	$t_i > 2$	7%	38%	35%	14%	4%	2%
p1	$t_i > 5$	19%	54%	20%	5%	1%	1%
p2	$t_i > 2$	8%	35%	35%	14%	5%	3%
p2	$t_i > 5$	21%	50%	21%	5%	2%	1%

Having a large share of one-strip clusters implies the disadvantage that the analog readout cannot be exploited and thereby the resolution becomes worse.

The lower row of Fig. 9 shows the simulated η-distributions for different selection cuts on the signal-to-noise ratio $(s/n)_i$ of a single strip. The comparison with the upper row of Fig. 9 (data)

shows qualitatively a good agreement. The edges become smoother with increasing threshold.

7. Cluster sizes

Another property characterizing a cluster is its width, i.e. the number of detector strips belonging to that cluster. Table 1 shows typical examples of cluster width distributions of two double-sided detectors. The n-sides are named n1 (with intermediate strips) and n2 (without intermediate strips). Both p-sides (p1 and p2) are equipped with intermediate strips. Results for two different selection cuts on the strip significance t_i are shown.

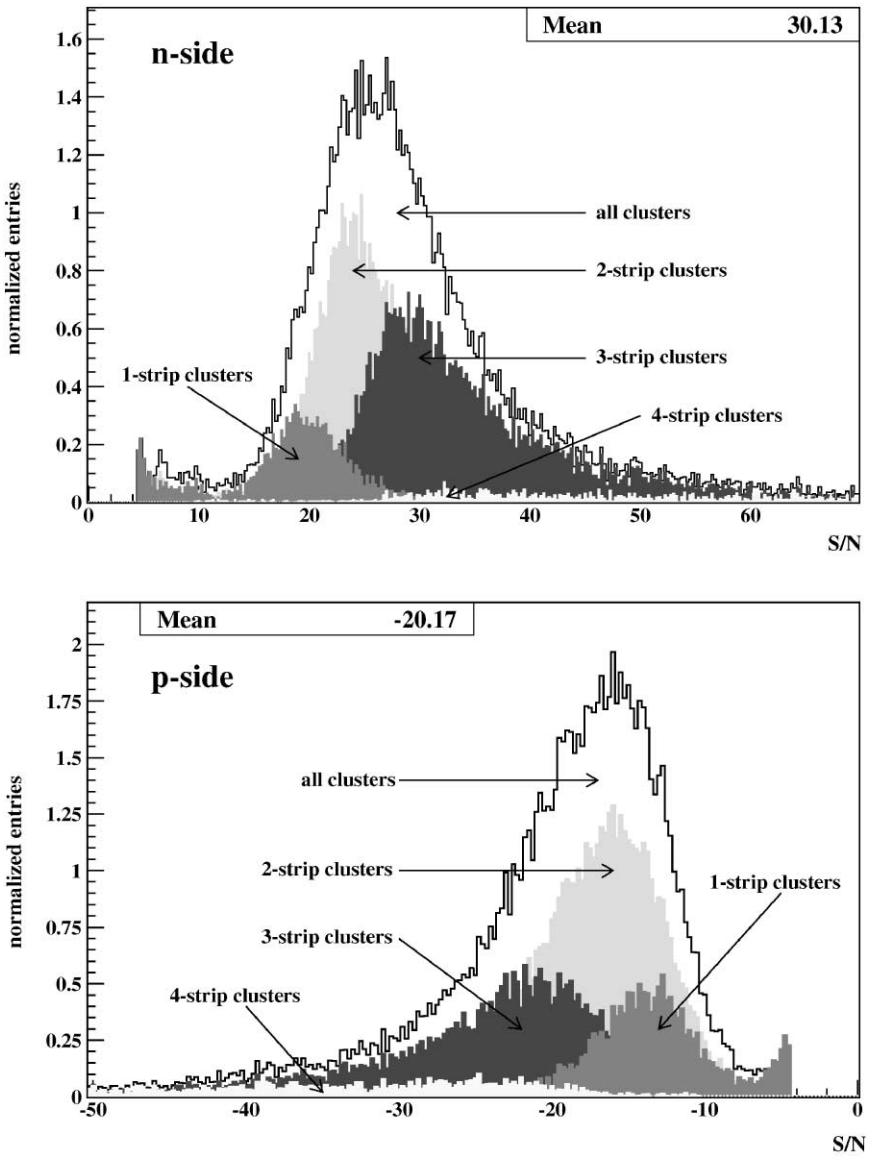

Fig. 10. Signal-to-noise distributions for clusters of different widths.

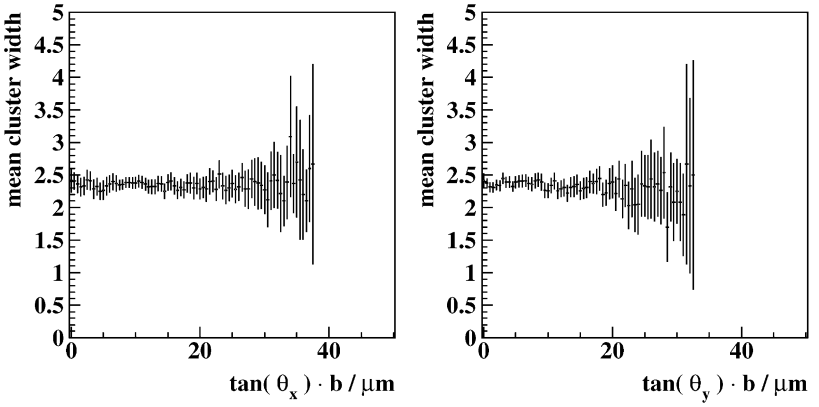

Fig. 11. Shows the mean cluster width as a function of the inclination angles θ_x and θ_y which are given as tan θ times the detector depth of $b = 280$ μm. This quantity is a measure of the transverse size of the charge distribution generated by the particles. The data are taken from a detector n-side mounted in superlayer 5 quadrant 3 of the VDS.

Three factors prove to be important to explain the observed cluster width distributions:

(1) the signal-to-noise of the detectors,
(2) the selection cut on the strip significance t_i,
(3) the capacitive coupling between adjacent strips.

The influence of the signal-to-noise becomes apparent when comparing n- and p-sides. The n-sides have a signal-to-noise of $S/N = 25$ (peak position) and the p-sides of $S/N = 16$. This explains why the p-sides have a lower share of 3- and 4-strip clusters, but a higher share of 1- and 2-strip clusters than the n-sides. In Fig. 10 the signal-to-noise distributions of clusters with different widths are shown.

The cut on the strip significance t_i has huge impact. The higher is the cut the higher is the share of 1- and 2-strip clusters. The cut on the cluster significance T has only negligible influence on the cluster width distribution (below 1%-point [15]). In the analysis presented here we used a cut of $T > 15$.

The capacitive coupling between the detector strips is essential to explain the high shares of 3- and 4-strip clusters, otherwise there would be basically only 1- and 2 strip-clusters. The model calculation shows that the coupling between two adjacent readout strips is about 5–8%, which agrees well with the design specifications.

There are three other factors which influence the cluster width distributions and were examined in this study, but proved to be less important in the case of HERA-B conditions: the strip pitch, the inclination angle of the tracks and the operation voltage. Fig. 11 shows that the mean cluster width remains constant as a function of the inclination angles (θ_x, θ_y) of the tracks.

8. Conclusions

The properties of the HERA-B silicon microstrip detectors are well understood. Cluster shape and cluster size distributions are well described by a model which was derived from a study of data obtained from a laser test stand. This agreement confirms the possibility to study properties of silicon strip detectors with laser beams in the laboratory and to apply these results to an environment of minimum ionizing particles.

References

[1] T. Lohse, et al. (HERA-B Collaboration), An Experiment to Study CP Violation in the B System Using an Internal

Target at the HERA Proton Ring, HERA-B Proposal, DESY-PRC 94/02, 1994.
[2] R.H. Richter et al., Nucl. Instr. and Meth. A 377 (1996) 412.
[3] A. Bischoff et al., Nucl. Instr. and Meth. A 326 (1993) 27.
[4] I. Abt et al., Nucl. Instr. and Meth. A 439 (1999) 442.
[5] L. Evensen, T. Westgaard, Nucl. Instr. and Meth. A 392 (1997) 206.
[6] I. Abt et al., Nucl. Instr. and Meth. A 411 (1998) 191.
[7] C. Bauer et al., Nucl. Instr. and Meth. A 447 (2000) 61.
[8] W. Wagner, Nucl. Instr. and Meth. A 446 (2000) 222.
[9] C. Bauer et al., Nucl. Instr. and Meth. A 453 (2000) 103.
[10] W. Fallot-Burghardt, et al., HELIX 128-x User Manual, HD-ASIC-33-0697, Version 2.1, Heidelberg, 1999.
[11] I. Kisel, S. Masciocchi, CATS: A Cellular Automaton for Tracking in Silicon, HERA-B Internal Note 99–242, 1999.
[12] I. Kisel et al. (NEMO collaboration), Nucl. Instr. and Meth. A 387 (1997) 433.
[13] M. Schmelling, The HOLMES Program Package, HERA-B-99-086 internal note.
[14] I. Abt et al., Nucl. Instr. and Meth. A 423 (1999) 303.
[15] W. Wagner, Auswertung der Daten des HERA-B Vertexdetektors im Hinblick auf die physikalischen Eigenschaften der verwendeten Siliziumstreifenzähler, Dissertation, Munich, 1999.